Agrobiodiversity
Open Access

ARTICLE
https://doi.org/10.48130/abd-0025-0011
Agrobiodiversity **2025**, 2(4): 78–88

Mechanistic insights into the antagonistic effects of *Trichoderma hamatum* Z32 against root rot pathogens revealed by genomic and metabolomic analyses

Neng Yang[1,2,3#], Honglin Zhang[1,2,3#], Yuzhou Feng[3], Chaojun Shi[4], Jinhui Jiang[1,2,3], Yinbiao Zhou[1,2,3], Jiahao Jia[1,2,3], Lương Hùng Tiến[5], Hoàng Trung Tín[5], Xiaoyu Xu[1*], Shengchao Yang[2,3,6*] and Tao Liu[1,2,3*]

[1] *College of Agronomy and Biotechnology, Yunnan Agricultural University, Kunming 650201, China*
[2] *National Local Joint Engineering Research Center for Germplasm Innovation and Utilization of Chinese Medicinal Materials in Southwest Yunnan Agricultural University, Kunming 650201, China*
[3] *Yunnan Key Laboratory of Medicinal Plant Biology, Yunnan Agricultural University, Kunming 650201, China*
[4] *College of Tobacco Science, Yunnan Agricultural University, Kunming 650201, China*
[5] *Faculty of Agronomy, Thai Nguyen University of Agriculture and Forestry, Thai Nguyen, Vietnam*
[6] *College of Biological and Agricultural Sciences, Honghe University, Mengzi 661199, China*
[#] These authors contributed equally: Neng Yang, Honglin Zhang
[*] Corresponding authors, E-mail: 1431740754@qq.com; shengchaoyang@163.com; yantao618@126.com

Abstract

Root rot in *Panax notoginseng* is primarily caused by *Fusarium oxysporum*. A rhizosphere-derived *Trichoderma hamatum* strain, Z32, was isolated and evaluated for its biocontrol potential. Dual culture assays showed that Z32 inhibited *F. oxysporum*'s growth by 62%, and microscopy revealed hyphal coiling, indicating competition-based antagonism. Genome sequencing produced a 42.69 Mb assembly with 10,837 predicted genes, including 451 carbohydrate-active enzyme (CAZyme) genes involved in cell wall degradation. Ten biosynthetic gene clusters related to antimicrobial metabolites were identified, and metabolomic profiling confirmed multiple antifungal and growth-promoting compounds. These findings reveal that *T. hamatum* Z32 suppresses soilborne pathogens through diverse mechanisms, providing a promising and environmentally friendly strategy for controlling root rot in *P. notoginseng*.

Citation: Yang N, Zhang H, Feng Y, Shi C, Jiang J, et al. 2025. Mechanistic insights into the antagonistic effects of *Trichoderma hamatum* Z32 against root rot pathogens revealed by genomic and metabolomic analyses. *Agrobiodiversity* 2(4): 78–88 https://doi.org/10.48130/abd-0025-0011

Introduction

Panax notoginseng is a valuable medicinal plant with high economic importance[1]. However, its cultivation and industrial development are severely threatened by pathogenic fungi[2]. Among these diseases, root rot is particularly destructive, often resulting in severe yield losses or even complete crop failure, thereby imposing substantial economic burdens on the *P. notoginseng* industry[3]. These studies have stated that *Fusarium* fungi are the main cause of the disease[4,5]. Although the main treatment of root rot is chemical methods, using too much of these chemicals will seriously damage the environmental balance and endanger agricultural security[6]. In response to the growing awareness of these ecological risks, biological control agents (BCAs) have gained increasing attention as promising and eco-friendly alternatives for managing soilborne diseases[7]. Beneficial microorganisms inhibit harmful pathogens and promote plant growth by increasing soil microbial diversity and changing the interactions among microorganisms, ultimately making the microbial community around the root zone stronger and more resistant[8]. *Trichoderma* is widely recognized as having important biological control capabilities[9]. However, the molecular mechanisms underlying their antifungal activities and their precise contributions to disease suppression remain insufficiently understood, limiting their broader application in sustainable agriculture. Therefore, identifying and studying microbial opponents that specifically attack harmful soil pathogens is important for us to develop strong and lasting biological control strategies.

Among the various microorganisms used for biological control, strains of the genus *Trichoderma* have attracted special attention because they are so powerful that they can suppress soilborne diseases and help plants grow better[10]. *Trichoderma hamatum*, a representative member of the family *Hypocreaceae*, is particularly noted for its broad-spectrum biocontrol efficacy and plant growth-promoting capabilities[11]. In addition to fighting pathogens, *T. hamatum* has a host of other powerful skills. It can be antibacterial[11], be antioxidant[12], drive away insects[13], inhibit weed growth[14], and help plants grow better[15]. Members of the genus *Trichoderma* are ubiquitously distributed in diverse ecological niches, particularly in rhizosphere soils, agricultural environments, and habitats enriched with decomposing plant residues or organic matter[16]. *Trichoderma* species are widely used as biocontrol agents because they can suppress or antagonize plant pathogens. They use several methods to deal with these threats, such as taking nutrients and territory, infecting other fungi, releasing biologically active chemicals, and strengthening the defense system of the host plant[17]. There is a key process called mycoparasitism, which means that *Trichoderma*'s mycelium actively finds harmful fungi and eats them. During this process, hydrolytic enzymes such as chitinases and β-1,3-glucanases are produced, which degrade fungal cell walls and show strong activity against *Ascomycota* species[18]. In addition to enzymatic degradation, *Trichoderma* produces various antimicrobial secondary metabolites that contribute to its biocontrol activity. For instance, *T. harzianum* synthesizes sesquiterpenes and aspinolides via polyketide pathways, which exhibit strong antifungal effects[19]. In addition, transcriptome analysis found that during the parasitic stage, genes responsible for producing cell wall-degrading enzymes and membrane transporters are expressed in large quantities, revealing the molecular mechanism of fungal parasitic interactions[20]. Niche competition also represents an important antagonistic strategy used by *Trichoderma*. By rapidly colonizing infection sites, exploiting available nutrients, and occupying ecological niches, *Trichoderma* effectively restricts the proliferation of soilborne pathogens[16]. Collectively, these diverse antagonistic mechanisms highlight the ecological versatility of

Trichoderma and underscore its potential as an effective and sustainable biocontrol agent in agricultural systems.

Different *Trichoderma* strains have shown strong biological control capabilities when dealing with plant diseases caused by *Fusarium*. Certain *Trichoderma* strains, including *T. asperellum*, *T. harzianum*, and *T. atroviride*, have been shown to suppress pathogens caused by *Fusarium* species such as *F. solani*, *F. oxysporum*, *F. graminearum*, and *F. sporotrichioides*[21,22]. However, the considerable variability in antagonistic efficacy among different *Trichoderma* strains underscores the importance of strain-specific screening to ensure effective biocontrol outcomes. For example, *in vitro* assays have shown that certain *Trichoderma* strains can significantly suppress the mycelial growth of *Fusarium* through direct antagonistic interactions such as hyphal overgrowth and enzymatic degradation, achieving inhibition rates as high as 82.62%[23]. Despite these encouraging findings, the antimicrobial mechanisms of *Trichoderma* against *F. oxysporum* remain incompletely understood, largely because of genetic variation and mechanistic diversity among strains. This knowledge gap highlights the need for systematic investigations that integrate genomics, metabolomics, and functional analyses to unravel strain-specific antifungal strategies. This study highlights the practical importance of *Trichoderma* in crop production, demonstrating its potential as an environmentally friendly and effective approach for pest management.

The genus *Trichoderma* exhibits remarkable genetic diversity, which is primarily reflected in extensive variations and polymorphisms within its genome sequences. Comparative genomic studies have revealed notable differences in genome size among *Trichoderma* strains. For instance, *T. harzianum* CBMAI-0711 possesses a genome of approximately 32 Mb, whereas other strains such as Th3844 (40 Mb), Th0179 (39 Mb), and *T. atroviride* CBMAI-00020 (36 Mb) show substantial variation, underscoring both intra- and interspecific genomic diversity[24]. Genome mining has further demonstrated structural variation at the level of biosynthetic gene clusters (BGCs). For example, the recently described species *T. agriamazonicum* contains 33 BGCs, of which 27 remain uncharacterized[25]. These clusters encode polyketides and other metabolites associated with cell wall degradation, including proteins involved in lignin and chitin breakdown. Such genetic variation provides a molecular basis for the metabolic flexibility and phenotypic plasticity that enable *Trichoderma* species to adapt to diverse ecological niches and exert broad-spectrum antagonistic effects.

Therefore, studying the genetic structure of *Trichoderma* can help us better understand why it suppresses *Fusarium* species, the main antagonists responsible for root rot in *P. notoginseng*. For this research, we specifically obtained a strain called *T. hamatum* from the soil around the roots of a particularly well-growing *P. notoginseng*. Its antagonistic potential against *F. oxysporum* was evaluated using a five-point dual culture assay, and physical interactions between the two fungi were further characterized by scanning electron microscopy (SEM). To gain deeper mechanistic insights, we adopted a metabologenomics approach, integrating whole-genome sequencing and assembly with untargeted metabolomic profiling[26–29]. Comparative genomic annotation was subsequently performed to identify biosynthetic gene clusters and secondary metabolites associated with antifungal activity.

The study wanted to see if *T. hamatum* could deal with *Fusarium* spp., the chief culprit in causing *P. notoginseng* to rot. It is also necessary to understand why it can suppress these bacteria and find the reasons from a genetic and biochemical perspective. By broadening the genomic understanding of *Trichoderma* species, this study deepens current insights into their biology and provides a foundation for developing sustainable biocontrol strategies against root rot in *P. notoginseng*. Moreover, this work offers valuable data for phylogenetic and functional genomic studies of *T. hamatum*, thereby advancing our understanding of its biocontrol mechanisms and evolutionary adaptations.

Materials and methods

Cultivation of *T. hamatum* Z32

The *T. hamatum* strain Z32, isolated from the rhizosphere soil of healthy *P. notoginseng*, is preserved in the Southwest Microbial Germplasm Resource Bank at Yunnan Agricultural University. For culture revival, the strain was first grown on potato dextrose agar (PDA) plates at 28 °C for approximately one week to allow the formation of dense mycelial mats. Agar plugs from these plates were then transferred into potato dextrose broth (PDB) and incubated under shaking at 200 rpm for about seven days to promote sporulation. The resulting culture was filtered to collect spores, which were flash-frozen in liquid nitrogen and stored at −80 °C for subsequent experiments.

Dual culture assay

To evaluate whether *T. hamatum* Z32 could inhibit the growth of *F. oxysporum*, both strains were simultaneously inoculated onto PDA plates in a dual culture confrontation assay. The extent of inhibition was assessed using a five-level rating scale. In each plate, a single plug of *F. oxysporum* was placed at the center, and five agar plugs containing the strain Z32 were distributed evenly around it. The control (CK) contained only the pathogen and no antagonistic fungus. To ensure experimental reliability, three biologically independent assays were conducted, each comprising three parallel technical replicates. After incubation at 28 °C for approximately 72 hours, the antagonistic activity of *T. hamatum* Z32 was evaluated by measuring the radial growth of *F. oxysporum* and the width of the clear inhibition zone formed between the two colonies. The inhibition ratio (%) was calculated according to the following formula:

$$\text{Inhibition rate} = \frac{(R_0 - R_1)}{R_0} \times 100\%$$

In the inhibition rate formula, R_0 corresponds to the mean radial growth of *F. oxysporum* colonies under control conditions, and R_1 refers to the radius of the colony obtained when *F. oxysporum* was cultured with the antagonistic strain Z32.

Scanning electron microscopy observation of the antagonistic region

The morphological interactions between *T. hamatum* strain Z32 and *F. oxysporum* were examined using SEM. For the control treatment (CK), only *F. oxysporum* was cultured on the PDA medium. In contrast, the experimental plates were co-inoculated with both fungi to enable direct mycelial contact. Small circular agar sections (approximately 0.5 cm in diameter) were cut from the region where the two colonies met and used for microscopic preparation.

Samples for SEM were prepared following standard fixation and dehydration procedures. Agar blocks were washed three times with 0.1 M phosphate-buffered saline (PBS) (pH 7.4) for 15 min per wash, then fixed with 1% osmium tetroxide (OsO_4) in PBS for 1–2 hours at room temperature in the dark. After fixation, samples were washed again in PBS and dehydrated in a graded ethanol series (30%–100%), followed by immersion in isoamyl acetate and critical-point drying. The dried specimens were mounted on aluminum stubs with conductive carbon tape, sputter-coated with gold (~30 s), and examined using a ZEISS Gemini Sigma 300 SEM (Jena, Germany).

Molecular characterization of *T. hamatum* Z32

Genomic DNA of *T. hamatum* Z32 was extracted via the cetrimonium bromide (CTAB) method. The internal transcribed spacer (ITS) region was amplified using the primers ITS1/ITS4 with polymerase chain reaction (PCR) conditions of 94 °C for 10 min, then 35 cycles of 94 °C

for 30 s, 54 °C for 30 s, and 72 °C for 30 s, followed by a final 10-min extension at 72 °C. Finally, the sample was heated at 72 °C for another 10 min to allow all the DNA to replicate. After purifying the PCR products, we performed Sanger sequencing using the primer pair ITS1/ITS4 (produced by Shanghai Shenggong Biotechnology Co., Ltd. completed). In order to determine the species of the fungi, we compared the detected sequence data with the NCBI ITS database using a BLAST search.

Genomic analysis: sequencing and assembly procedures

For genome assembly, *T. hamatum* Z32 was analyzed using a hybrid sequencing approach that merged high-fidelity short reads with long-read data to ensure both accuracy and continuity in the final assembly. For short-read sequencing, a reference database was first built according to the procedure outlined in[30]. We sequenced the *T. hamatum* Z32 genome using the DNBSEQ-T7 system (MGI, China), generating paired-end reads of 150 nucleotides (PE150).

For long-read sequencing, we used the PacBio Revio platform and prepared libraries following the SMRTbell Express Template Prep Kit 2.0 protocol (Pacific Biosciences). About 15 μg of high-quality genomic DNA was first treated to remove single-stranded overhangs, repair damage, polish ends, and add A-tails. The processed fragments were then ligated with T-tailed SMRTbell adapters at 20 °C for roughly 60 min.

We purified the ligated DNA library and assessed its fragment length and concentration using the FEMTO Pulse and Qubit instruments. Roughly 3 μg of the library was then size-selected on a BluePippin device to remove fragments smaller than 15 kb, followed by an additional round of purification and quantification. The final library was annealed with sequencing primers, mixed with Sequel II DNA polymerase at a concentration of 120 pM, and loaded onto an 8 M SMRT Cell via diffusion. We carried out sequencing on the Sequel II system for a runtime of about 1,800 min, generating long reads of 15–20 kilobases. Frasergen Bioinformatics (Wuhan, China) handled all library preparation and sequencing procedures.

Genome assembly was performed at the contig level using Hifiasm. The assembled genome was analyzed to determine the nucleotide composition (A, G, C, T, N) and overall GC content. To evaluate the genome's completeness and coverage consistency, sequencing reads generated from both short- and long-read technologies were aligned back to the assembly with BWA and Minimap2. Metrics including the mapping rate, genome coverage, and depth distribution were calculated. Coverage depth was computed for each genomic position, and a nonoverlapping 1,000-bp sliding window (or the full length for shorter contigs) was used to calculate the average sequencing depth and GC content per window. These data were visualized in density plots of GC content versus sequencing depth to evaluate GC bias and potential contamination.

The genome's completeness was further assessed using Benchmarking sets of Universal Single-Copy Orthologs (BUSCO) with the fungi_odb10 database, reporting metrics for completeness, fragmentation, and gene loss based on single-copy orthologs from OrthoDB. We used Merqury to estimate the assembly's quality value (QV) by comparing k-mer profiles derived from the genome assembly and the sequencing reads. We reported the genome size along with other assembly quality indicators and submitted the raw sequencing datasets to NCBI, accessible via BioProject PRJNA1163295 and BioSample SAMN43845003.

Prediction of the genome's composition

To annotate transfer RNA genes, the *T. hamatum* Z32 genome was analyzed with tRNAscan-SE. Ribosomal RNA (rRNA) genes were predicted with RNAmmer (v1.2). In addition, microRNA (miRNA) and small nuclear RNA (snRNA) sequences were predicted using covariance models from the Rfam database (rfam.org) via the INFERNAL software included in Rfam. We evaluated the completeness of the genome assembly with BUSCO, using single-copy orthologs derived from OrthoDB. At the same time, antiSMASH (version 7.0) was applied to detect and characterize gene clusters associated with secondary metabolite production.

Comparative genomic analysis

To investigate genetic differences between *T. hamatum* Z32 and seven other *Trichoderma* strains, and to confirm the taxonomic identity of Z32, protein sequences from all eight strains were clustered according to sequence similarity using the OrthoFinder2 pipeline. Pairwise protein sequence similarities were computed with DIAMOND, and orthologous groups were identified by OrthoFinder2. Sequences from each single-copy homologous gene family were first aligned using MUSCLE. The resulting alignments were subsequently concatenated to generate a comprehensive supergene alignment in PHYLIP format.

We used RaxML's maximum likelihood method to infer the kinship between species. To determine when they were separated, we used r8s and MCMCtrees in the PAML suite to calibrate the evolutionary tree on the basis of fossil data and timelines published in studies such as TimeTree. The CAFE tool helped us analyze changes in gene family size according to orthogroup classification and identify those groups with significant changes. These groups were functionally annotated through Gene Ontology (GO) and Kyoto Encyclopedia of Genes and Genomes (KEGG) pathway enrichment, and statistical significance was adjusted with the false discovery rate (FDR) to avoid errors caused by multiple comparisons.

We analyzed each single-copy homologous gene family shared across species with the branch-site model in codeml (PAML suite) to detect the signatures of positive selection.

Functional annotation and genomic analysis

We annotated the protein-coding genes of *T. hamatum* Z32 by comparing their sequences with the NR, KEGG, Clusters of Orthologous Groups (COG), GO, and Swiss-Prot databases. Functional predictions were performed by aligning proteins with BLASTp in Diamond (version 0.9.12.113). For GO classification, InterProScan (version 5.50-84.0) was used to assign relevant annotations.

Carbohydrate-active enzymes (CAZymes) were analyzed using the dbCAN2 process, which combines dbCAN-HMMdb V7 and HMMER (version 3.1b2). CAZymes were analyzed following the standard dbCAN2 workflow. A stringent E-value of 1×10^{-15} and a minimum coverage of 0.35 were applied to filter the sequences. Antimicrobial resistance proteins were then identified by aligning the predicted sequences to the comprehensive antibiotic resistance database (CARD) database (v3.0.1) with Diamond BLASTp, retaining only the top-scoring alignment for each query. Virulence factors were annotated by alignment against the database of fungal virulence factors (DFVF) and pathogen–host interactions database (PHI) protein databases (E-value $\leq 1 \times 10^{-5}$), with the highest scoring hits retained.

Signal peptides indicative of secreted proteins were predicted using SignalP (v4.1), and transmembrane helices were identified using TMHMM (v2.0c), which applies a hidden Markov model to detect transmembrane regions.

Secondary metabolite analysis and identification

For metabolomic profiling, 50 μL of each sample was mixed with 150 μL of an extraction solvent containing an internal standard (acetonitrile–methanol, 1:4, v/v). The mixture was vortexed for 3 min and centrifuged at 12,000 rpm and 4 °C for 10 min. A 150-μL aliquot of the supernatant was transferred to a fresh tube, frozen at −20 °C for 30 min, and centrifuged again under the same conditions for 3 min. Subsequently, 120 μL of the clarified supernatant was loaded into autosampler vial

inserts for liquid chromatography–mass spectrometry (LC-MS) analysis, with all steps performed on ice to preserve the metabolites' integrity.

Chromatographic separation was conducted using a Waters ACQUITY Premier HSS T3 column (1.8 µm, 2.1 × 100 mm) with Solvent A (0.1% formic acid in water) and Solvent B (0.1% formic acid in acetonitrile). The column temperature was maintained at 40 °C, with a flow rate of 0.4 mL/min and an injection volume of 4 µL. Analyses were performed in both positive and negative ionization modes. The elution gradient started at 5% B, increased to 20% B over 2 min, then to 60% B within 3 min; after that, it increased further to 99% B in 1 minute (held for 1.5 min), returned to 5% B in 0.1 min, and equilibrated for 2.4 min.

Mass spectrometry was carried out on a Sciex system using Analyst TF software (v1.7.1) in information-dependent acquisition (IDA) mode. The source conditions were nebulizer gas 1 (GAS1) = 50 psi, heater gas 2 (GAS2) = 50 psi, curtain gas (CUR) = 25 psi, and temperature (TEM) = 550 °C. Declustering voltages were set at 60 V (positive) and −60 V (negative), whereas the ion spray voltages were 5,000 V and −4,000 V, respectively. Time-of-flight mass spectrocopy (TOF MS) scans covered m/z 50–1,000 with 200 ms of accumulation time, and product ion scans ranged from m/z 25–1,000 with 40 ms of accumulation time. The collision energy was ±30 V with a 15-V spread, unit resolution, a charge state of 1, and an intensity threshold of 100 cps. Isotopes within 4 Da were excluded, the mass tolerance was 50 ppm, and the number of candidate ions per cycle was limited. Raw data were converted to mzXML format using ProteoWizard.

Data were processed using XCMS for peak detection, alignment, and correction of retention time. Peaks missing in over 50% of samples were removed, and the remaining missing values were imputed via the k-nearest neighbors (KNN) method. Peak areas were normalized using support vector regression (SVR). Metabolites were annotated according to internal and public databases, prediction libraries, and metDNA technology. Quality control (QC) samples with coefficient of variation (CV) < 0.3 were used to assess data quality, and only metabolites with identification scores of > 0.5 and CV < 0.3 in the QC samples were retained. When combining positive and negative ion datasets, the metabolites with the lowest CVs were prioritized to ensure reliability.

Statistical analysis

We calculated the mean and standard deviation for each measurement and carried out statistical analyses using SPSS software (version 27.0, IBM, Armonk, NY, USA).

Results

Evaluation of the inhibitory effects of *T. hamatum* Z32

In the five-point dual culture assay, *T. hamatum* Z32 effectively inhibited *F. oxysporum*, producing a clearly visible inhibition zone with diffuse yet well-defined edges (Fig. 1c). Quantitative analysis showed an inhibition rate of 62% (Supplementary Table S1). The results showed that strain Z32 has strong antifungal properties, and it may have used several methods to prevent the growth of fungi, such as releasing biologically active secondary metabolites and seizing their common living space.

The SEM examination found that after *F. oxysporum* grew together with *T. hamatum* Z32, its physical structure changed significantly. Under monoculture conditions, the hyphae of both *F. oxysporum* and *T. hamatum* Z32 exhibited intact structures with smooth surfaces (Fig. 2a, b). In contrast, co-culture conditions induced pronounced hyphal shrinkage and surface wrinkling in *F. oxysporum* (Fig. 2c). These structural deformations suggest that strain Z32 exerts antagonistic effects, likely through mechanisms such as nutrient competition and occupation of ecological niches. Collectively, the SEM observations provide further evidence that *T. hamatum* Z32 effectively suppresses the growth of *F. oxysporum*.

Genomic features of *T. hamatum Z32*

High-precision (HiFi) sequencing of *T. hamatum* strain Z32 generated 7.35 Gb of raw data, with an average sequencing depth of 172.2 times the genome size. After quality control, a total of 376,147 high-quality reads were retained (Supplementary Table S2). By integrating HiFi reads with Hi-C data, the *T. hamatum* Z32 genome was reconstructed into 20 contigs totaling 42.69 Mb, with an N50 of 6.74 Mb and a GC content of 46.26% (Fig. 3; Supplementary Table S3). Mapping the sequencing reads back to the assembly yielded a high alignment rate of 98.36% and genome coverage of 99.96%, demonstrating the robustness of the assembly. BUSCO analysis indicated that 98.6% of the core conserved genes were fully represented, confirming the high quality and reliability of the genome assembly and providing a solid basis for subsequent functional and comparative genomic studies (Supplementary Table S4).

Genome feature identification and annotation

The *T. hamatum* Z32 genome contains 12,137 protein-coding genes, with an average gene length of 2,589 bp and an average coding sequence (CDS) length of 1,242 bp. Each of these genes has an average of 2.46 exons, and the average lengths of the exons and introns are 505.15 and 923.51 bp, respectively (Supplementary Table S5). The genome of *T. hamatum* Z32 contains 450 noncoding RNAs (ncRNAs), including 221 transfer RNAs (tRNAs), 204 ribosomal RNAs (rRNAs), and 25 small nuclear RNAs (snRNAs) (Table 1).

The function annotation process used databases such as InterPro, GO, KEGG, SwissProt, TrEMBL and NR, and the specific information is presented in Table S6. Among the predicted genes in *T. hamatum* Z32, 7,943 (about 73.3%) were classified into the three principal GO categories: Biological processes, cellular components, and molecular functions. Biological processes were the most abundant, with genes

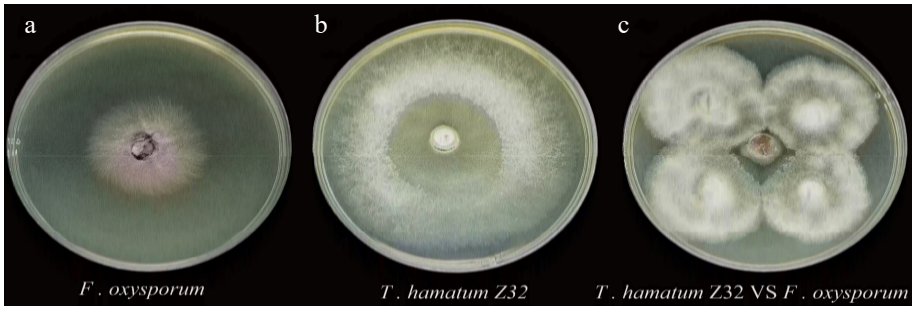

Fig. 1 Individual cultures and dual culture assay of *T. hamatum* Z32 and *F. oxysporum*.

(**a**) *F. oxysporum* cultured alone (pathogen control); (**b**) *T. hamatum* Z32 cultured alone (antagonist control); (**c**) dual culture plate showing *F. oxysporum* inoculated at the center and *T. hamatum* Z32 inoculated at four peripheral points.

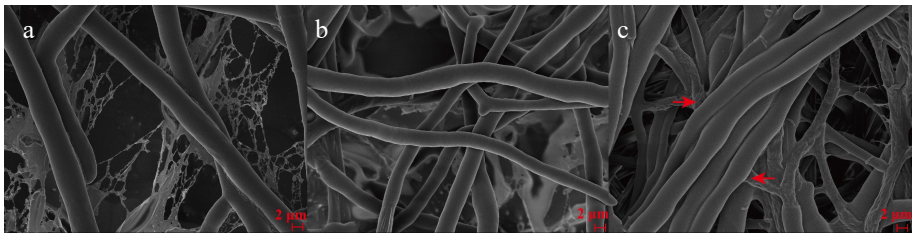

Fig. 2 Electron microscope images taken using scanning technology were recorded and used to show the surface and structural characteristics of the antimicrobial species.

(**a**) *F. oxysporum*; (**b**) *T. hamatum* Z32; (**c**) co-culture of *F. oxysporum* and *T. hamatum* Z32. The arrows mark where *T hamatum* Z32 interacts with harmful fungi, and we can see that *T hamatum* Z32's mycelium entangles the pathogen. This entanglement can cause the pathogen's mycelium to wither and shrink, and can also cause structural damage through resistance.

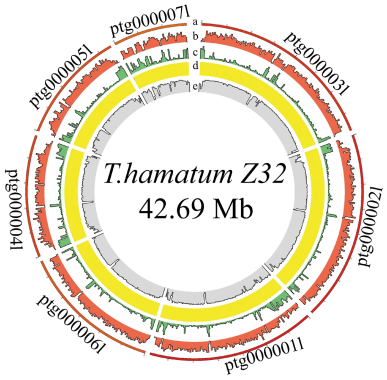

Fig. 3 Circos plot displaying the genome of *T. hamatum* Z32.

From outermost to innermost, the concentric rings represent contigs, gene density, repeat sequences, noncoding RNAs (ncRNAs), and GC content. Although the genome assembly includes 20 contigs, only the 7 longest are shown, as the shorter contigs contribute little or no gene information.

Table 1. ncRNA statistics and composition in *T. hamatum* Z32.

Type	Copy	Average length (bp)	Total length (bp)	% of genome
miRNA	0	0.00	0	0.00
tRNA	221	87.54	19,346	0.05
rRNA	204	2,209.75	450,790	1.06
18S	75	1,794.55	134,591	0.32
28S	79	3,929.13	310,401	0.73
5S	50	115.96	5,798	0.01
snRNA	25	138.20	3,455	0.01
CD-box	14	129.14	1,808	0.00
hypermethylated allele-coxA associated (HACA)-box	3	170.33	511	0.00
splicing	8	142.00	1,136	0.00
scaRNA	0	0.00	0	0.00

predominantly involved in metabolic activities, cellular functions, and processes occurring in single organisms (Supplementary Fig. S1). KEGG pathway analysis revealed that 4,157 genes (38.36%) belong to the five major pathway classes, with metabolism-related pathways forming the largest group, particularly those associated with carbohydrate, amino acid, and lipid metabolism (Supplementary Table S6; Supplementary Fig. S2).

Comparative genomic analysis

By conducting a phylogenetic analysis of 1,884 single-copy orthologically conserved genes, we inferred the evolutionary relationships among the eight *Trichoderma* species and one outgroup strain, as shown in Fig. 4. The analysis estimated the divergence time from the outgroup, *Saccharomyces cerevisiae* S288C, at approximately 424 million years ago (MYA). Within the *Trichoderma* genus, *T. hamatum* diverged from *T. asperelloides* and *T. asperellum* CBS433.97 about 6 MYA, whereas *T. asperelloides* and *T. asperellum* CBS433.97 separated from each other around 2 MYA (Fig. 4).

Evolutionary analysis of the nine fungal species showed that gene family contractions were more frequent than expansions (Fig. 4). In *Trichoderma*, *T. hamatum*, *T. asperelloides*, and *T. asperellum* CBS433.97 exhibited expansions in 70, 16, and 48 gene families, respectively, whereas contractions were observed in 80, 62, and 26 gene families, respectively.

Analysis of enzyme production potential in *T. hamatum* Z32

CAZymes are essential for diverse biological processes in *Trichoderma* species, particularly their mycoparasitic lifestyle. Genomic analysis of *T hamatum* Z32 with the dbCANseq database found that it has 451 genes responsible for encoding CAZymes. The predicted genome of *T. hamatum* Z32 contains genes assigned to six major CAZyme families: 252 glycoside hydrolases (GHs), 13 carbohydrate-binding modules (CBMs), 73 auxiliary activity enzymes (AAs), 25 carbohydrate esterases (CEs), 78 glycosyltransferases (GTs), and 10 polysaccharide lyases (PLs). Specific data can be seen in Fig. 5. Among these, GHs constituted the largest CAZyme family.

In addition, annotation against the PHI-base database revealed 4,706 genes associated with pathogen–host interactions (Supplementary Table S7). Most of these genes are associated with weaker toxicity (2,086 genes), followed by genes that do not affect pathogenicity (1,953 genes), and finally those that lead to loss of pathogenicity (264 genes) (Fig. 6; Supplementary Table S7).

Examining the gene assembly for producing secondary metabolites in *T. hamatum Z32*

We used antiSMASH software (v7.1.0) to analyze the genome of *T. hamatum* Z32 to find genes that produce secondary metabolites. It was found that 29 such gene clusters were distributed across nine scaffolds (Supplementary Table S8). The *T. hamatum* Z32 genome contains 15 biosynthetic gene clusters (BGCs) related to nonribosomal peptide synthetases (NRPSs) and NRPS-like variants, 2 clusters corresponding to Type I polyketide synthases, and 7 clusters associated with terpene synthesis. To evaluate the strain's biocontrol potential, 10 of these BGCs were linked to previously characterized secondary metabolites, with their predicted chemical structures and genomic locations summarized in Fig. 7.

Among them, three BGCs exhibited 100% amino acid sequence homology with characterized clusters: Region 1.2 of *Ptg1* encodes an NRPS cluster responsible for peramine biosynthesis (Fig. 7b), Region 2.2 of *Ptg2* encodes an NRPS-like cluster related to choline biosynthesis (Fig. 7f), and Region 4.3 of *Ptg4* harbors NRPS and T1PKS clusters involved in 1,3,6,8-tetrahydroxynaphthalene biosynthesis (Fig. 7j). Additionally, the cluster located in Region 7.1 (*Pgt7*, NRPS) showed

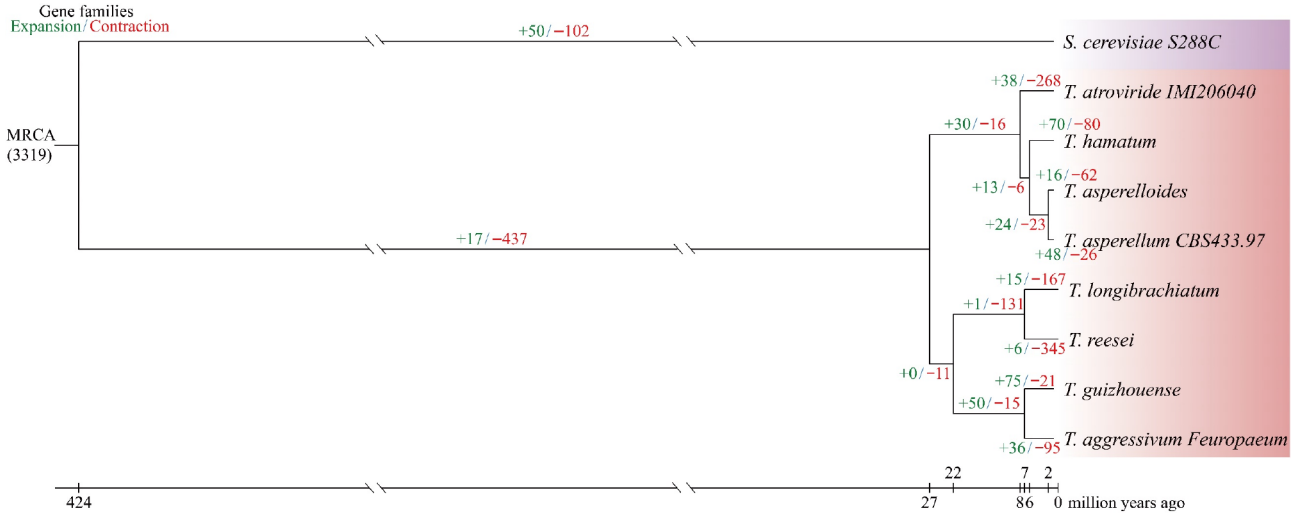

Fig. 4 A maximum likelihood phylogenetic tree was generated using 1,884 single-copy orthologs from eight *Trichoderma* strains and one outgroup.
All nodes were supported with 100% bootstrap values, and branch lengths indicate the estimated divergence times in millions of years ago (MYA). For each species, green and red numbers denote gene family expansions and contractions, respectively, while the background color reflects the corresponding taxonomic group.

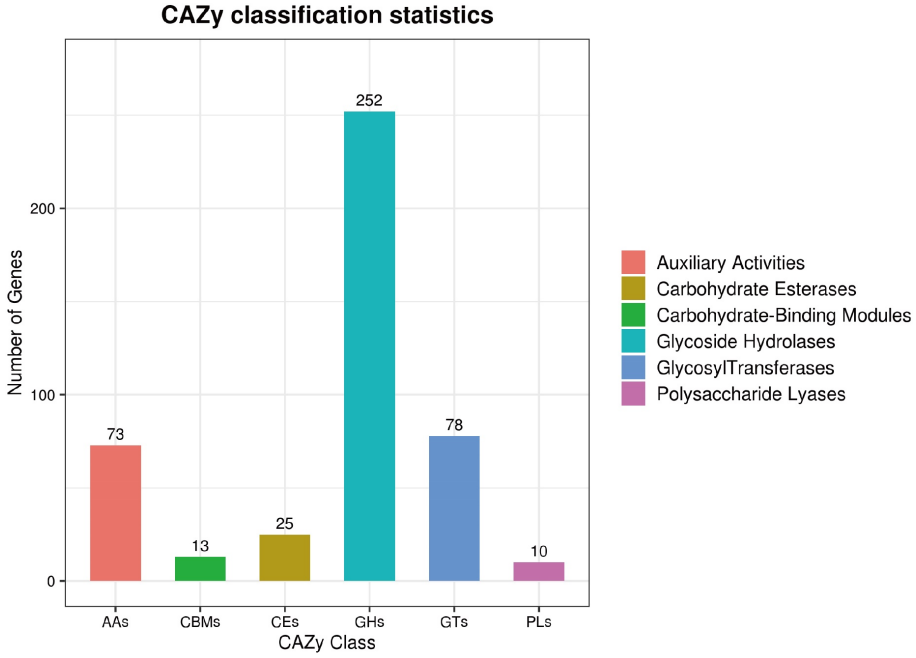

Fig. 5 The predicted CAZyme genes in *T. hamatum* Z32 were grouped into different families.
In the *T. hamatum* Z32 genome, the identified genes were categorized into six main CAZyme families: auxiliary activities (AAs), carbohydrate esterases (CEs), carbohydrate-binding modules (CBMs), glycoside hydrolases (GHs), glycosyltransferases (GTs), and polysaccharide lyases (PLs).

75% sequence similarity to the melinacidin IV biosynthetic cluster (Fig. 7a). Other identified clusters were predicted to participate in the biosynthesis of ascochlorin (Fig. 7c), fumonisin B1 (Fig. 7d), curvupallide-B (Fig. 7e), fusaric acid (Fig. 7g), leucinostatin A (Fig. 7h), and metachelin C (Fig. 7i).

Secondary metabolite analysis of *T. hamatum* Z32

To validate the predicted secondary metabolites via BGC analysis, non-targeted metabolomic profiling was performed on the fermentation broth of *T. hamatum* Z32. In total, 5,883 secondary metabolites were detected (Supplementary Table S9), with amino acids and their derivatives accounting for the largest fraction (26.99%), followed by benzene and its substituted derivatives, which comprised 15.84% of the identified compounds (Supplementary Fig. S3). In addition, diverse compound classes were detected, including indole derivatives (e.g., indole-3-carbinol, naltrindole), choline-related compounds (e.g., choline, dehydrocorydaline), terpenoids, and phenolic acids (e.g., ferulic acid).

Principal component analysis (PCA) was performed to assess the overall metabolic variation among *T. hamatum* Z32 samples. The first two principal components, PC1 and PC2, explained 66.08% and 18.52% of the total variance, respectively, capturing the major metabolic differences. The QC samples are closely clustered together in the two-dimensional score plot, proving that this analytical method is both stable and reliable. Within the treatment group, two of the three biological replicates clustered closely, whereas one replicate

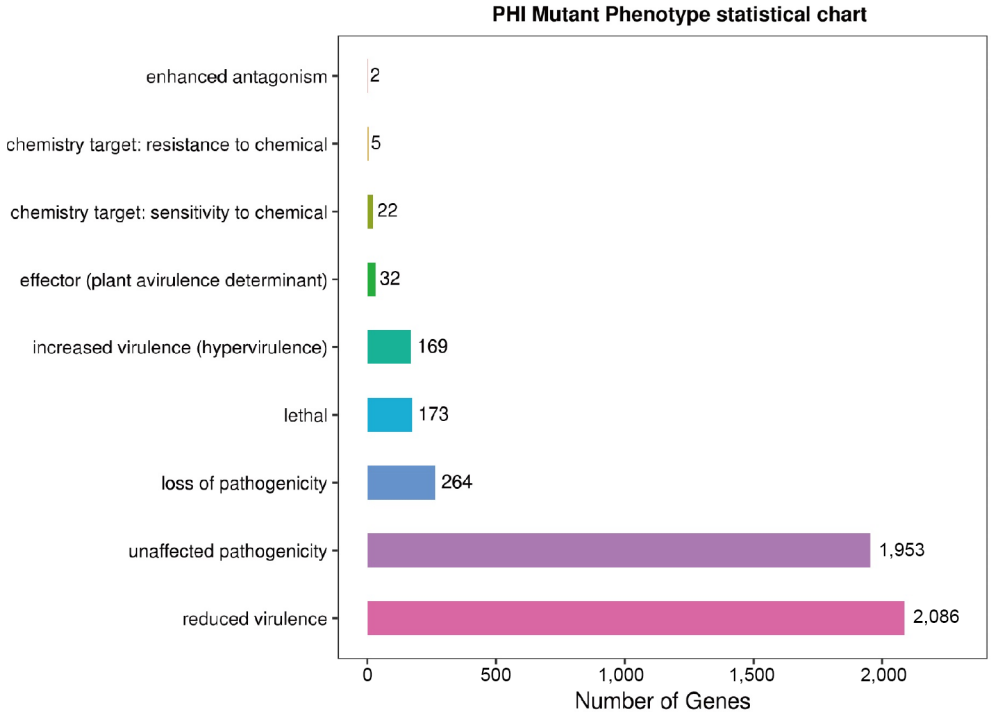

Fig. 6 The figure shows the distribution of pathogen–host interaction (PHI) mutation phenotypes, with nine mutation types along the vertical axis and the corresponding number of annotated genes on the horizontal axis.

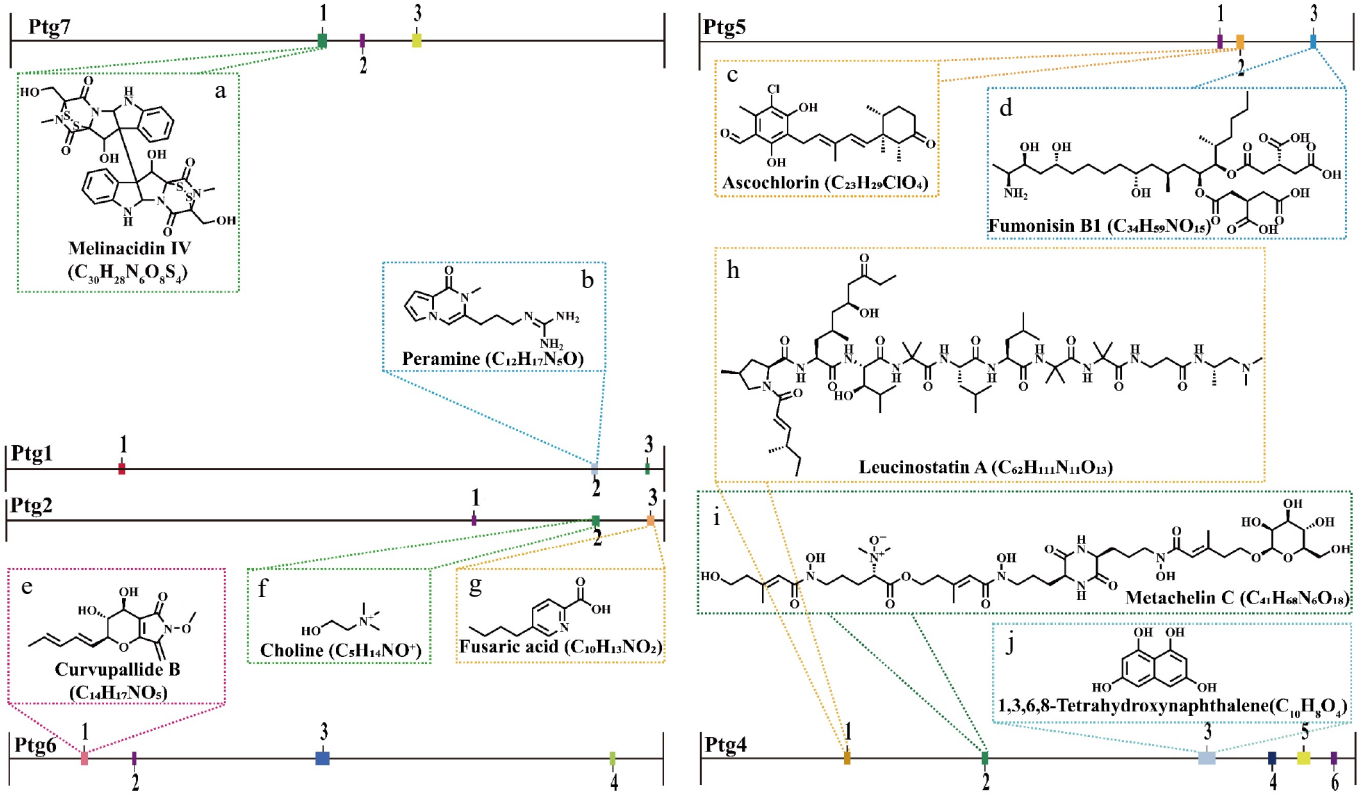

Fig. 7 The secondary metabolite biosynthetic gene clusters identified in the *T. hamatum* Z32 genome using antiSMASH (version 7.0).

The predicted compounds associated with each cluster are: (**a**) Melinacidin IV ($C_{30}H_{38}N_4O_5S_4$), (**b**) peramine ($C_{12}H_{17}N_5O$), (**c**) ascochlorin ($C_{23}H_{29}ClO_4$), (**d**) fumonisin B1 ($C_{34}H_{59}NO_{15}$), (**e**) curvupallide B ($C_{14}H_{17}NO_5$), (**f**) choline ($C_5H_{14}NO^+$), (**g**) fusaric acid ($C_{10}H_{13}NO_2$), (**h**) leucinostatin A ($C_{62}H_{111}N_{11}O_{13}$), (**i**) metachelin C ($C_{41}H_{68}N_6O_{18}$), and (**j**) 1,3,6,8-tetrahydroxynaphthalene ($C_{10}H_8O_4$).

showed a slight deviation in its principal component space, potentially reflecting inherent metabolic variation or differential treatment responses. Nevertheless, the overall within-group variation was markedly smaller than the between-group variation, supporting the reliability and interpretability of the metabolomic dataset (Supplementary Fig. S4).

Discussion

F. oxysporum is the main pathogen responsible for root rot in *P. notoginseng*, representing a major challenge to the sustainable cultivation of this medicinal plant[31]. Currently, disease management largely depends on chemical fungicides[32]; however, their widespread use has caused unintended consequences, including pesticide residues and the emergence of fungicide-resistant microbial populations[33]. These problems show that we are in urgent need of safer and more effective alternatives than traditional chemical treatments[34]. Under such conditions, biological control strategies have attracted considerable attention because of their safety, environmental friendliness, and sustainability[35]. The expanding use of microbial inoculants, particularly fungal biocontrol strains, underscores the need for effective and dependable biocontrol agents (BCAs) within sustainable plant disease management programs[36].

There are a variety of microorganisms in the soil around plant roots, among which bacteria that help plant growth, known as plant growth-promoting rhizobacteria (PGPRs), have been the most widely studied. They can make plants grow better[37], stimulate plant defense responses[38], and suppress harmful bacteria in the soil[39]. Studies have found that using PGPRs can greatly reduce reliance on artificial fertilizers and pesticides, as these not only protect the ecological balance but also reduce harm to human health[40].

Trichoderma fungi are recognized as vital members of the PGPR community. When they establish themselves in plant roots, they can alter the microbial landscape of the rhizosphere, enrich populations of beneficial fungi, and enhance plants' tolerance of soils contaminated by heavy metals such as cadmium and mercury[41]. In addition to fostering plant growth through mechanisms like phosphate solubilization[11] and nitrogen fixation[42], these fungi produce a variety of antimicrobial compounds that help suppress pathogenic microorganisms[43]. Among them, *T. hamatum* stands out for its ability to generate diverse secondary metabolites that specifically inhibit plant pathogens, demonstrating considerable potential as an environmentally sustainable biocontrol agent[44].

In the case of *P. notoginseng*, a *T. hamatum* strain isolated from its rhizosphere exhibited strong antagonistic activity against root rot. Laboratory experiments showed that this strain effectively curtailed the growth of *F. oxysporum*, the primary pathogen behind the disease (Supplmentary Table S1). The combination of broad-spectrum antagonism and plant growth-promoting properties positions *Trichoderma* species as key contributors to sustainable agriculture, and they are increasingly recognized as valuable tools for eco-friendly disease management strategies[17].

To explore the genomic characteristics of the biocontrol fungus *T. hamatum* Z32, we performed comprehensive whole-genome sequencing followed by comparative genomic analyses. The assembled genome was subsequently compared with those of seven other *Trichoderma* species and one outgroup strain to elucidate its evolutionary relationships and functional attributes. According to the results of evolutionary tree analysis, strain Z32 has the closest genetic relationship with *T. asperelloides* and *T. asperellum* CBS43397. Comparative analysis revealed significant gene family dynamics, with 70 families that have expanded and 80 families that have contracted (Fig. 4). GO enrichment analysis revealed that in *T. hamatum* Z32, the expanded gene families were primarily enriched in metabolic pathways associated with phenylpropanoid metabolism, particularly those involved in ferulic acid conversion and cinnamic acid degradation (Supplementary Fig. S5a). As cinnamic, ferulic, and p-hydroxycinnamic acids, key intermediates in plant secondary metabolism, are derived from the phenylpropanoid pathway, the capacity of strain Z32 to convert or degrade these compounds may contribute to its plant growth-promoting effects. In contrast, the contracted gene families were mainly enriched in transmembrane transporter activity (Supplementary Fig. S5b), potentially affecting the strain's capacity to utilize environmental resources or metabolic products. KEGG pathway enrichment analysis indicated that the expanded gene families of *T. hamatum* Z32 were primarily associated with the lysine biosynthetic pathway (Supplementary Fig. S5c). This pathway likely plays a pivotal role in the organism's metabolism, potentially facilitating increased lysine accumulation, enhanced metabolic flexibility, and improved adaptability under diverse environmental or symbiotic conditions. Conversely, the contracted families were enriched in sulfur metabolism (Supplementary Fig. S5d), which may reduce the organism's sulfur utilization efficiency and constrain its ecological adaptability. Notably, previous studies have reported that *T. guizhouense* exhibits strong plant growth-promoting and biocontrol capabilities[41], and the high genomic similarity between Z32 and *T. guizhouense* (Supplementary Fig. S6) further supports the substantial biocontrol potential of this strain.

Trichoderma fungi can directly fight plant pathogens. They have several methods: They can parasitize other fungi, make antibacterial substances[45], release enzymes that destroy cell walls[46], and compete for territory in root-zone ecosystems. These antagonistic activities are closely linked to the functional genes encoded within *Trichoderma* genomes[32]. In line with this, SEM revealed that hyphal coiling by Z32 induced the shrinkage and breakage of *F. oxysporum* hyphae. Similar mechanisms have been widely documented. Zhang et al.[47]reported that the suppression of *F. oxysporum* by *T. harzianum* E5 primarily results from direct physical interaction. During this process, the hyphae of *T. harzianum* coil around the pathogen's mycelia, thereby restricting its growth and proliferation. Rees et al.[48]demonstrated that *T. hamatum* suppresses *Armillaria mellea* through hyphal coiling and coverage, completely inhibiting the pathogen's growth. Similarly, Zhang et al.[49]observed that *T. hamatum* exhibits parallel hyphal growth and coiling around *Sclerotinia* spp., leading to hyphal deformation, shrinkage, and breakage. Taken together, these findings, together with our observations, suggest that *T. hamatum* Z32 likely suppresses *F. oxysporum* through a combination of hyphal coiling and robust competitive growth.

Genomic functional annotation, antagonistic assays, and electron microscopy collectively indicated that *T. hamatum* possesses significant potential to suppress pathogenic fungi through mycoparasitism. On the molecular scale, secondary metabolites in plants are important for resisting pathogens because of their antibacterial ability. Genetic analysis of genes related to secondary metabolites showed that *T. hamatum* Z32 contains 29 BGCs and can produce five major categories of secondary metabolites. These include alkaloids (such as peramine and fusaric acid), amine derivatives (such as choline), polyketides (such as 1,3,6,8-tetrahydroxyphthalene, ascochlorin, fumonisin B1), NRPS-derived peptides (such as melinacidin IV, curvupallide-B, leucostatin A, and metachelin C), and siderophores (such as metachelin C).

Previous studies have demonstrated that alkaloids exhibit broad-spectrum antifungal activity against diverse plant pathogens, including *Fusarium* spp.[50]. Polyketides, such as wailupemycins M–P and bikaverin, have been reported to inhibit both phytopathogenic fungi (e.g., *Fusarium* spp.) and oomycetes (e.g., *Phytophthora*)[51]. Similarly, nonribosomal peptides, including cyclic lipopeptides and fusaric acid derivatives, display potent antifungal activity and can markedly suppress the radial growth of *F. oxysporum*[51]. Moreover, siderophores derived from *Pseudomonas stutzeri* exhibit strong antagonistic effects against *F. oxysporum*[52]. Taken together, these findings support the hypothesis that BGC-derived secondary metabolites produced by *T. hamatum* Z32 may contribute substantially to its inhibitory activity against *F. oxysporum*.

Through genomic analysis and verification of existing research results, we speculated that the inhibitory effect of this strain may be related to its secondary metabolites; however, direct experimental validation of their functional roles is still lacking. Thus, the current results indicate only a potential association rather than a definitive causal relationship. Moreover, given that metabolite expression may exhibit dynamic changes under different culture conditions, the predictions may be subject to certain biases. Future research will focus on the following aspects: (1) Purification and isolation of key secondary metabolites; (2) *in vitro* antifungal assays to verify the biological functions of individual compounds; (3) determination of whether the antifungal activity of this strain is indeed attributable to these metabolites, in conjunction with the activity of hydrolytic enzymes; and (4) integration of transcriptomic and metabolomic data to elucidate the molecular mechanisms linking metabolite biosynthesis with their functional roles, thereby providing a comprehensive understanding of their contribution to the antagonistic activity of this strain.

In *T. hamatum* Z32, a total of 451 carbohydrate-active enzymes (CAZymes) were identified through genome annotation. The majority were glycoside hydrolases (252), followed by glycosyltransferases (78) and auxiliary activity enzymes (73), indicating a diverse enzymatic repertoire involved in carbohydrate metabolism. This enzyme composition suggests that Z32 possesses strong potential for carbohydrate degradation and modification, which may underlie its interactions with host plants and its capacity to suppress pathogens. GHs, as components of plant defense systems, can catalyze specific reactions that contribute to pathogen resistance[53].

Integration with nontargeted metabolomic analysis of Z32 fermentation broth further revealed the presence of bioactive metabolites with antimicrobial potential, including choline derivatives, triterpenoids, and indole-related compounds. Choline compounds have been reported to participate in osmoregulation and metabolic processes, indirectly enhancing plants' stress tolerance[54]. Triterpenoids serve as key components of plant defense, providing protection either directly through inhibition of herbivorous pests or indirectly via modulation of ecological interactions[55]. Indole and its derivatives exhibit broad-spectrum bioactivities, including antifungal and insecticidal effects, and can promote plant growth and development[56]. Collectively, these genomic and metabolomic features suggest that *T. hamatum* Z32 employs multiple molecular mechanisms to enhance plant health and suppress pathogenic fungi.

The genomic evidence suggests that *T. hamatum* Z32 can generate diverse secondary metabolites through several key biosynthetic routes, including NRPS-like, terpene, NRPS, and T1PKS pathways. The diverse metabolic pathways identified in *T. hamatum* Z32 likely form the biochemical basis of its antagonistic activity against pathogens and may also contribute to the enhanced tolerance and vigor in the host plants. For instance, terpenoid volatiles can function as herbivore-induced plant volatiles (HIPVs), mediating tritrophic interactions among plants, herbivores, and natural enemies[57]. In addition, some plants generate structurally complex metabolites through NRPS–terpene hybrid gene clusters, potentially providing synergistic enhancement of defense capabilities[58]. The enrichment of TPS-a and TPS-b genes in *T. hamatum* may represent an adaptive mechanism that broadens its terpenoid biosynthetic potential and enhances chemical diversity. These include monoterpenes, sesquiterpenes, and diterpenes, allowing organisms to better cope with complex biological challenges[59]. Metabolites produced by T1PKS gene clusters, as reported in fungi such as *Sarcopodium* sp., appear to contribute to the activation of plant defense responses. These findings suggest that T1PKS-associated pathways could be further explored for developing environmentally sustainable biofertilizers and biological control strategies[60].

Given its rich repertoire of biosynthetic gene clusters and secondary metabolism-associated genes, *T. hamatum* Z32 appears to be well suited for use as a biocontrol agent against root rot in *P. notoginseng*. However, the present study primarily evaluated its biocontrol potential at the genomic and metabolomic levels, without field validation or direct assessment of the cytotoxic effects of compounds such as fumonisin B1 and fusaric acid on plants. Future studies should focus on comprehensive field efficacy evaluations and further advance the development and optimization of biocontrol formulations based on *T. hamatum* Z32.

Conclusions

We found a strain of *T. hamatum* called Z32, which is particularly powerful and can effectively fight the bad fungus *F. oxysporum*. Strain Z32 effectively inhibited the growth of *F. oxysporum*, the main pathogen responsible for root rot in *P. notoginseng*. Dual culture experiments revealed an inhibition rate of about 62%. Under microscopy, Z32 hyphae were observed to intertwine and wrap around the pathogen's filaments, a behavior consistent with mycoparasitic activity. The genome of *T. hamatum* Z32 (42.69 Mb; 20 contigs; N50 of 6.74 Mb; GC content of 46.26%) contained 10,837 predicted genes, including CAZymes such as glycoside hydrolases, as well as multiple secondary metabolite biosynthetic gene clusters, highlighting its potential for biocontrol. Comparative phylogenomic analysis with seven other *Trichoderma* species revealed 70 expanded and 80 contracted gene families. Untargeted metabolomic profiling identified 5,883 metabolites, including indole derivatives (e.g., indole-3-methanol and indole-3-lactic acid) associated with plant growth regulation, and several antifungal compounds (e.g., choline, dehydrocorydaline, and ferulic acid). Our results provide insights into the genetic and biochemical factors underlying the biocontrol activity of *T. hamatum* Z32 and suggest its potential for developing environmentally friendly strategies to manage root rot in *P. notoginseng*. As some findings are derived from *in silico* analyses, experimental verification is necessary to confirm its effectiveness against *F. oxysporum*.

Author contributions

The authors confirm their contributions to the paper as follows: conceptualization and experimental design: Liu T, Yang S, Xu X, Yang N; data collection: Yang N, Zhang H, Feng Y, Shi C, Zhou Y, Jia J, Tiên LH, Tín HT; data analysis and interpretation: Yang N, Zhang H, Jiang J, Shi C, Tiên LH, Tín HT; manuscript drafting: Yang N. All authors reviewed the results and approved the final version of the manuscript.

Data availability

All research outputs from this work are openly available. The *T. hamatum* Z32 genome is accessible through NCBI (BioProject: PRJNA1163295; BioSample: SAMN43845003), and the raw metabolomics data have been deposited at the China National Center for Bioinformation (CNCB) under Project No. PRJCA046955, OMIX ID OMIX012064.

Acknowledgments

We thank all authors and mentors for their valuable support in data analysis and manuscript preparation. Funding This research was funded by The Sino-Vietnamese International Joint Laboratory for Characteristic & Cash Crops Green Development of Yunnan Province (202403AP140013), the National Key Research and Development (2021YFD1601003), and Yunnan Provincial Joint Funds for Agriculture General Program(202301BD070001-198).

Conflict of interest

The authors declare that they have no conflict of interest.

Supplementary information accompanies this paper at (https://www.maxapress.com/article/doi/10.48130/abd-0025-0011)

Dates

Received 1 July 2025; Revised 17 October 2025; Accepted 7 November 2025; Published online 27 November 2025

References

1. Wei G, Zhang G, Li M, Zheng Y, Zheng W, et al. 2024. *Panax notoginseng*: panoramagram of phytochemical and pharmacological properties, biosynthesis, and regulation and production of ginsenosides. *Horticulture Research* 11:uhae170
2. Su L, Li W, Chen X, Wang P, Liu D. 2024. Proline-rich protein PRPL1 enhances *Panax notoginseng* defence against *Fusarium solani* by regulating reactive oxygen species balance and strengthening the cell wall barrier. *Plant, Cell & Environment* 47:2375–93
3. Yang Y, Wei F, Li Z, Han F, Guan H, et al. 2023. Improper crop rotation may enrich soil-borne pathogens of *panax notoginseng*. *Journal of Phytopathology* 171:567–76
4. Zhou X, Luo C, Li K, Zhu D, Jiang L, et al. 2022. First report of *Fusarium striatum* causing root rot disease of *Panax notoginseng* in yunnan, China. *Phyton-International Journal of Experimental Botany* 91:13–20
5. Lin C, Feng XL, Liu Y, Li ZC, Li XZ, et al. 2023. Bioinformatic analysis of secondary metabolite biosynthetic potential in pathogenic *Fusarium*. *Journal of Fungi* 9:850
6. Wen T, Xie P, Liu H, Liu T, Zhao M, et al. 2023. Tapping the rhizosphere metabolites for the prebiotic control of soil-borne bacterial wilt disease. *Nature Communications* 14:4497
7. Ali Sulaiman M, Bello SK. 2024. Biological control of soil-borne pathogens in arid lands: a review. *Journal of Plant Diseases and Protection* 131:293–313
8. Liu Y, Zhang H, Wang J, Gao W, Sun X, et al. 2024. Nonpathogenic *pseudomonas syringae* derivatives and its metabolites trigger the plant "cry for help" response to assemble disease suppressing and growth promoting rhizomicrobiome. *Nature Communications* 15:1907
9. Wang W, Wang H, Zhang Z, Li W, Yin X, Long Y. 2024. Dual RNA sequencing during *Trichoderma harzianum-Phytophthora capsici* interaction reveals multiple biological processes involved in the inhibition and highlights the cell wall as a potential target. *Pest Management Science* 80:4533–42
10. Harman GE, Howell CR, Viterbo A, Chet I, Lorito M. 2004. *Trichoderma* species — opportunistic, avirulent plant symbionts. *Nature Reviews Microbiology* 2:43–56
11. Contreras-Cornejo HA, Schmoll M, Esquivel-Ayala BA, González-Esquivel CE, Rocha-Ramírez V, et al. 2024. Mechanisms for plant growth promotion activated by *Trichoderma* in natural and managed terrestrial ecosystems. *Microbiological Research* 281:127621
12. Wang Z, Wang Z, Lu B, Quan X, Zhao G, et al. 2022. Antagonistic potential of *Trichoderma* as a biocontrol agent against *Sclerotinia asari*. *Frontiers in Microbiology* 13:997050
13. Lana M, Simón O, Velasco P, Rodríguez VM, Caballero P, et al. 2023. First study on the root endophytic fungus *Trichoderma hamatum* as an entomopathogen: Development of a fungal bioinsecticide against cotton leafworm (*Spodoptera littoralis*). *Microbiological Research* 270:127334
14. Bansal R, Sahoo SA, Barvkar VT, Srivastava AK, Mukherjee PK. 2023. *Trichoderma virens* exerts herbicidal effect on *Arabidopsis thaliana* via modulation of amino acid metabolism. *Plant Science* 332:111702
15. Lodi RS, Peng C, Dong X, Deng P, Peng L. 2023. *Trichoderma hamatum* and its benefits. *Journal of Fungi* 9:994
16. Tao C, Wang Z, Liu S, Lv N, Deng X, et al. 2023. Additive fungal interactions drive biocontrol of Fusarium wilt disease. *New Phytologist* 238:1198–214
17. Woo SL, Hermosa R, Lorito M, Monte E. 2023. *Trichoderma*: a multipurpose, plant-beneficial microorganism for eco-sustainable agriculture. *Nature Reviews Microbiology* 21:312–26
18. Wang CY, Gan D, Li CZ, Zhang SQ, Li BX, et al. 2022. A new highly oxygenated polyketide derivative from *Trichoderma* sp. and its antifungal activity. *Chemistry & Biodiversity* 19:e202200671
19. Cardoza RE, McCormick SP, Izquierdo-Bueno I, Martínez-Reyes N, Lindo L, et al. 2022. Identification of polyketide synthase genes required for aspinolide biosynthesis in *Trichoderma arundinaceum*. *Applied Microbiology and Biotechnology* 106:7153–71
20. Yu SF, Sun ZB, Li SD, Hu YF, Ren Q, et al. 2023. The adenylate cyclase-encoding gene *crac* is involved in *Clonostachys rosea* mycoparasitism. *Journal of Fungi* 9:861
21. Yazid SNE, Tajudin NI, Razman NAA, Selamat J, Ismail SI, et al. 2023. Mycotoxigenic fungal growth inhibition and multi-mycotoxin reduction of potential biological control agents indigenous to grain maize. *Mycotoxin Research* 39:177–92
22. Hernández-Melchor DJ, Guerrero-Chávez AC, Ferrera-Rodríguez MR, Ferrera-Cerrato R, Larsen J, et al. 2023. Cellulase and chitinase activities and antagonism against *Fusarium oxysporum* f. sp. cubense race 1 of six *Trichoderma* strains isolated from Mexican maize cropping. *Biotechnology Letters* 45:387–400
23. Nazir N, Badri ZA, Bhat NA, Bhat FA, Sultan P, et al. 2022. Effect of the combination of biological, chemical control and agronomic technique in integrated management pea root rot and its productivity. *Scientific Reports* 12:11348
24. Rosolen RR, Horta MAC, de Azevedo PHC, da Silva CC, Sforca DA, et al. 2023. Whole-genome sequencing and comparative genomic analysis of potential biotechnological strains of *Trichoderma harzianum, Trichoderma atroviride*, and *Trichoderma reesei*. *Molecular Genetics and Genomics* 298:735–54
25. Sales LS, Andrade JP, Santana LL, Santos Conceição TD, Neto DS, et al. 2025. Redefining the clade *Spirale* of the genus *Trichoderma* by re-analyses of marker sequences and the description of new species. *Fungal Biology* 129:101529
26. Feng XL, Zhang RQ, Wang DC, Dong WG, Wang ZX, et al. 2023. Genomic and metabolite profiling reveal a novel *Streptomyces* strain, QHH-9511, from the Qinghai-Tibet Plateau. *Microbiology Spectrum* 11:e0276422
27. Zhang RQ, Feng XL, Wang ZX, Xie TC, Duan Y, et al. 2022. Genomic and metabolomic analyses of the medicinal fungus *inonotus hispidus* for its metabolite's biosynthesis and medicinal application. *Journal of Fungi* 8:1245
28. Wei J, Cheng M, Zhu JF, Zhang Y, Cui K, et al. 2023. Comparative genomic analysis and metabolic potential profiling of a novel culinary-medicinal mushroom, *Hericium rajendrae* (Basidiomycota). *Journal of Fungi* 9:1018
29. Xie X, Zhao L, Song Y, Qiao Y, Wang ZX, et al. 2024. Genome-wide characterization and metabolite profiling of *Cyathus olla*: insights into the biosynthesis of medicinal compounds. *BMC Genomics* 25:618
30. Zhu X, Li S, Liu L, Li S, Luo Y, et al. 2020. Genome sequencing and analysis of *Thraustochytriidae* sp. SZU445 provides novel insights into the polyunsaturated fatty acid biosynthesis pathway. *Marine Drugs* 18:118
31. Nie H, Liao H, Wen J, Ling C, Zhang L, et al. 2024. *Foeniculum vulgare* essential oil nanoemulsion inhibits *Fusarium oxysporum* causing *Panax notoginseng* root-rot disease. *Journal of Ginseng Research* 48:236–44
32. Liu XY, Huo YY, Yang J, Li TT, Xu FR, et al. 2022. Integrated physiological, metabolomic, and proteome analysis of *Alpinia officinarum* Hance essential oil inhibits the growth of *Fusarium oxysporum* of *Panax notoginseng*. *Frontiers in Microbiology* 13:1031474
33. Li H, Yang J, Zhang X, Xu X, Song F, et al. 2022. Biocontrol of *Candida albicans* by antagonistic microorganisms and bioactive compounds. *antibiotics* 11:1238
34. Sa R, He S, Han D, Liu M, Yu Y, et al. 2022. Isolation and identification of a new biocontrol bacteria against *Salvia miltiorrhiza* root rot and optimization of culture conditions for antifungal substance production using response surface methodology. *BMC Microbiology* 22:231

35. Karačić V, Miljaković D, Marinković J, Ignjatov M, Milošević D, et al. 2024. *Bacillus* species: excellent biocontrol agents against tomato diseases. *Microorganisms* 12:457
36. Natsiopoulos D, Topalidou E, Mantzoukas S, Eliopoulos PA. 2024. Endophytic *Trichoderma*: potential and prospects for plant health management. *Pathogens* 13:548
37. Khosravi H, Khoshru B, Nosratabad AF, Mitra D. 2024. Exploring the landscape of biofertilizers containing plant growth-promoting rhizobacteria in Iran: Progress and research prospects. *Current Research in Microbial Sciences* 7:100268
38. Dunn MF, Becerra-Rivera VA. 2023. The biosynthesis and functions of polyamines in the interaction of plant growth-promoting rhizobacteria with plants. *Plants* 12:2671
39. Wang Y, Piao F, Di Y, Xu J, Wang Z, et al. 2024. *Serratia plymuthica* HK9-3 enhances tomato resistance against *Phytophthora capsici* by modulating antioxidant defense systems and rhizosphere micro-ecological condition. *Physiologia Plantarum* 176:e14323
40. Benchlih S, Esmaeel Q, Aberkani K, Tahiri A, Belabess Z, et al. 2023. Modes of action of biocontrol agents and elicitors for sustainable protection against bacterial canker of tomato. *Microorganisms* 11:726
41. Wang Y, Liu Z, Hao X, Wang Z, Wang Z, et al. 2023. Biodiversity of the beneficial soil-borne fungi steered by *Trichoderma*-amended biofertilizers stimulates plant production. *NPJ Biofilms and Microbiomes* 9:46
42. Li Y, Yang R, Häggblom MM, Li M, Guo L, et al. 2022. Characterization of diazotrophic root endophytes in Chinese silvergrass (*Miscanthus sinensis*). *Microbiome* 10:186
43. Xiao C, Li L, Liu Y, Huang Y, Wang Y, et al. 2022. Inhibitory effect and mechanism of *Trichoderma taxi* and its metabolite on *Trichophyton mentagrophyte*. *Journal of Fungi* 8:1006
44. Liu R, Chen M, Gao J, Luo M, Wang G. 2023. Identification of antagonistic fungi and their antifungal activities against aconite root rot pathogens. *Plant Signaling & Behavior* 18:2211852
45. Singh S, Singh AK, Pradhan B, Tripathi S, Kumar KS, et al. 2024. Harnessing *Trichoderma* mycoparasitism as a tool in the management of soil dwelling plant pathogens. *Microbial Ecology* 87:158
46. Akram S, Ahmed A, He P, He P, Liu Y, et al. 2023. Uniting the role of endophytic fungi against plant pathogens and their interaction. *Journal of Fungi* 9:72
47. Zhang F, Yang X, Ran W, Shen Q. 2014. *Fusarium oxysporum* induces the production of proteins and volatile organic compounds by *Trichoderma harzianum* T-E5. *FEMS Microbiology Letters* 359:116–23
48. Rees HJ, Bashir N, Drakulic J, Cromey MG, Bailey AM, et al. 2021. Identification of native endophytic Trichoderma spp. for investigation of in vitro antagonism towards Armillaria mellea using synthetic-and plant-based substrates. *Journal of Applied Microbiology* 131:392–403
49. Zhang H, Kong N, Liu B, Yang Y, Li C, et al. 2022. Biocontrol potential of *Trichoderma harzianum* CGMCC20739 (Tha739) against postharvest bitter rot of apples. *Microbiological Research* 265:127182
50. Huang BB, Gao MW, Li G, Ouyang MA, Chen QJ. 2023. Design, synthesis, structure–activity relationship, and three-dimensional quantitative structure–activity relationship of fusarium acid derivatives and analogues as potential fungicides. *Journal of Agricultural and Food Chemistry* 71: 18566–77
51. Macías-Rubalcava ML, Lappe-Oliveras P, Villanueva-Silva R. 2025. Disruption of cell wall and membrane integrity as antioomycete and antifungal mode of action by fusaric and 9, 10-dehydrofusaric acids from endophytic fungus *fusarium lactis* strain SME13-2. *Journal of Applied Microbiology* 136:lxae301
52. Karuppiah V, Natarajan S, Gangatharan M, Aldayel MF, Alsowayeh N, et al. 2022. Development of siderophore-based rhizobacterial consortium for the mitigation of biotic and abiotic environmental stresses in tomatoes: an *in vitro* and *in planta* approach. *Journal of Applied Microbiology* 133:3276–3287
53. Sivaramakrishnan M, Veeraganti Naveen Prakash C, Chandrasekar B. 2024. Multifaceted roles of plant glycosyl hydrolases during pathogen infections: More to discover. *Planta* 259:113
54. Zhang H, Li Y, Ling J, Zhao J, Li Y, et al. 2024. NRPS-like ATRR in plant-parasitic nematodes involved in glycine betaine metabolism to promote parasitism. *International Journal of Molecular Sciences* 25:4275
55. Mathur V, Dokka N, Raghunathan G, Rathinam M, Parashar M, et al. 2025. Beyond bitter: plant triterpenoids in the battle against herbivorous insects. *Journal of Experimental Botany* 76:4441–57
56. Wu Y, Sun A, Chen F, Zhao Y, Zhu X, et al. 2024. Synthesis, structure–activity relationship and biological evaluation of indole derivatives as anti-*Candida albicans* agents. *Bioorganic Chemistry* 146:107293
57. Wang W, Wang M, Feng J, Zhang S, Chen Y, et al. 2024. Terpene synthase gene family in Chinese chestnut (*Castanea mollissima* BL.) harbors two sesquiterpene synthase genes implicated in defense against gall wasp *Dryocosmus kuriphilus*. *Journal of Agricultural and Food Chemistry* 72:1571–81
58. Du Y, Li J, Chen S, Xia Y, Jin K. 2024. Pathogenicity analysis and comparative genomics reveal the different infection strategies between the generalist *Metarhizium anisopliae* and the specialist *Metarhizium acridum*. *Pest Management Science* 80:820–36
59. Wang Q, Jiang J, Liang Y, Li S, Xia Y, et al. 2025. Expansion and functional divergence of terpene synthase genes in angiosperms: a driving force of terpene diversity. *Horticulture Research* 12:uhae272
60. Zhang W, Ling M, Zhang K, Liu R, Huang X, et al. 2025. Complete genome sequence of the marine mangrove fungus *Sarcopodium* sp. QM3–1 confirmed its high potential for antimicrobial activity. *Marine Genomics* 79:101162